[CANCER RESEARCH (SUPPL.) 50, 1043s–1048s, February 1, 1990]

Dosimetric Model for Antibody Targeted Radionuclide Therapy of Tumor Cells in Cerebrospinal Fluid[1]

W. T. Millar[2] and A. Barrett

Department of Clinical Physics and Bioengineering [W. T. M.] and Radiation Oncology [A. B.], University of Glasgow, Beatson Oncology Center, Western Infirmary, Glasgow, Scotland

Abstract

Although encouraging results have been obtained using systemic radioimmunotherapy in the treatment of cancer, it is likely that regional applications may prove more effective. One such strategy is the treatment of central nervous system leukemia in children by intrathecal instillation of targeting or nontargeting β particle emitting radionuclide carriers. The β particle dosimetry of the spine is assessed, assuming that the spinal cord and the cerebrospinal fluid compartment can be adequately represented by a cylindrical annulus. The radionuclides investigated were ^{90}Y, ^{131}I, ^{67}Cu, and ^{199}Au. It is shown that the radiation dose to the cord can be significantly reduced using short range β particle emitters and that there is little advantage in using targeting carriers with these radionuclides. ^{199}Au and ^{67}Cu also have the advantage of having a suitable γ emission for imaging, permitting pretherapy imaging and dosimetric calculations to be undertaken prior to therapy. If these methods prove successful, it may be possible to replace the external beam component used in the treatment of central nervous system leukemia in children by intrathecal radionuclide therapy, thus reducing or avoiding side effects such as growth and intellectual impairment.

Introduction

The advent of monoclonal antibodies and radioimmunotherapy has encouraged the development of various protocols for systemic therapy of neoplastic disease. Specific and high affinity antibodies offer the potential of targeted radiation therapy, reducing the dose of nontargeted tissues (1–6). However, the specificity and cell density uptake of the labeled antibodies currently achieved (7) and the relatively slow kinetics of uptake limit the efficacy of such methods. Short range radionuclides with decay half-lives of the order of several hours; *e.g.*, the α particle emitters ^{211}At and ^{212}Bi are therefore unlikely to be useful in systemic therapy. The application of these methodologies to limited regional volumes such as in peritoneal infusion for ovarian cancer, isolated limb perfusion, and cerebrospinal fluid directed therapy could prove more successful. Lashford *et al.* (6) used intrathecal administration of ^{131}I-labeled monoclonal antibodies in the treatment of leptomeningeal disease from medulloblastoma with encouraging results. We have considered intrathecal β particle emitting radionuclide therapy in the treatment of central nervous system leukemia relapse in young children. This method would help to minimize radiation dose to nontargeted tissues (*e.g.*, brain, bone) while delivering sterilizing doses of radiation to cells in the meninges and the CSF.[3] Padova[4] has treated some patients with CNS leukemia. If effective, this form of treatment could be used for primary prevention of CNS disease or replace the external beam component of treatment for posterior fossa tumors. There would be a particular advantage in young children if this treatment could control disease since external beam radiotherapy with its effects on growth and intellectual function could be avoided. Whole body β particle dose will depend primarily on the stability of the radionuclide/carrier and the leakage of the radionuclide out of the CSF into the systemic circulation.

Many radioisotopes have been considered for radionuclide therapy, the particular choice being dependent on the clinical application, type of radiation emission, range, and lability of the radionuclide/carrier complex. ^{90}Y and ^{131}I have certainly been the more widely used although ^{67}Cu and ^{199}Au would appear to have suitable characteristics appropriate to short range β particle therapy as well as suitable γ emissions for imaging.

This paper considers the β particle dosimetry to the spine of intrathecally administered radionuclides coupled to targeting or nontargeting carriers, *i.e.*, a meningeal surface area or CSF volume distribution of radionuclide. The model used assumes that the spinal cord and cerebrospinal fluid space can be adequately represented by two concentric cylinders in the shape of an annulus.

Volume Distribution of Radionuclide. The spinal cord and the CSF were regarded as two concentric cylinders, with the volume between the cylindrical annulus containing the radionuclide (Fig. 1). Consequently the dose rate at any point can be determined by calculating the dose rate at that point due to the outer cylinder and subtracting the dose rate due to the inner cylinder where, in each case, the total cylindrical volume is filled with the radionuclide at the same concentration:

$$DR(x, t) = DR(x, t, R2) - \mathrm{DR}(x, t, R1)$$

where $DR(x, t)$ is the dose rate at point x due to the annulus and $DR(x, t, R)$ is the dose rate at point x due to a cylinder of radius R.

Using the MIRD formalism

$$DR(x, t, R1) = \Delta \mathrm{A}(t) \int_v \Phi(|\bar{x} - \bar{r}|)\, dV$$

where the integral is taken over the volume of the cylinder of radius $R1$ and $A(t)$ is the activity in μCi/ml at time t, Δ is the equilibrium dose constant (g-cGy/μCi-h), $|\bar{x} - \bar{r}|$ is the separation between point x and a point within the volume of integration, and $\Phi(|\bar{x} - \bar{r}|)$ is the specific absorbed dose fraction at point x due to a point source at r.

Following Berger (8), Φ can be written:

$$\Phi(z) = 4\pi\rho z^2 P_{90} F(\zeta)$$

where ρ is density of the medium (= 1), ζ is z/P_{90}, P_{90} is 90 percentile distance for the radionuclide, and $F(\zeta)$ is the scaled absorbed dose distribution.

The dose rate can then be written

$$DR(x, t, R1) = \frac{\Delta A(t)}{4\pi P_{90}} \int_v \frac{F(\zeta)}{z^2}\, dV$$

The actual dose $D(x, R1)$ can be found simply by integrating over the activity time course

$$D(x, R1) = \int_0^\infty DR(x, t, R1)\, dt$$

The function $F(\zeta)$ has been tabulated by Berger (8) at certain defined

[1] Presented at the "Second Conference on Radioimmunodetection and Radioimmunotherapy of Cancer," September 8–10, 1988, Princeton, NJ.

[2] To whom requests for reprints should be addressed, at the West of Scotland Health Boards, Department of Clinical Physics and Bioengineering, 11 West Graham St., Glasgow, Scotland.

[3] The abbreviations used are: CSF, cerebrospinal fluid; CNS, central nervous system.

[4] G. Padora, personal communication.

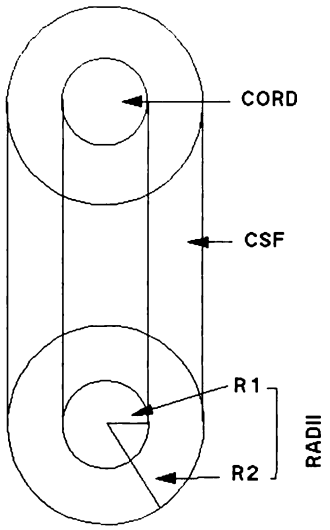

Fig. 1. Geometric model for CSF/CNS dosimetry.

values of ζ for a selection of different radionuclides. Calculation of the dose rate $DR(x, t)$ was carried out using numerical methods (Simpson's rule or gaussian quadrature). This requires the evaluation of $F(\zeta)$ at points not tabulated by Berger; these were obtained by interpolation using natural cubic spline representations of Berger's data. The natural choice of cylindrical coordinates for the elemental volume dV is not desirable since this leads to a singularity in the integrand when x is on the surface of the cylinder and potentially large computational errors very close to the surface. Consequently, spherical coordinates were used with the axes centered on point x. Further discussion can be found in Appendix 1.

Cylindrical Surface Area Distribution of Radionuclide. Assuming the radionuclide to be distributed uniformly on the surface of the cylinders in an infinitely thin thickness, then using the previous notation

$$DR(x, t) = DR(x, t, R1) + DR(x, t, R2)$$

In this case the dose rate is due to the summation of the two individual components and the total dose can be found as before.

$$DR(x, t, R1) = \Delta A(t) \int_S \Phi(|\bar{x} - \bar{r}|)\, dS$$

where S is over the surface of the cylinder. However, as x approaches the surface, *i.e.*, when x approaches the radius of the cylinder, large computational errors can occur close to the surface. Numerical integration and interpolation were carried out as for the volume distribution. Further discussion can be found in Appendix 2.

Results

The radionuclides considered here are ^{90}Y, ^{131}I, ^{67}Cu, and ^{199}Au. Computer programs were developed to calculate the dose rate distributions using the protocols discussed in Appendices 1 and 2. The scaled absorbed dose distribution for the radionuclides not tabulated by Berger (*i.e.*, ^{67}Cu, ^{199}Au) were computed using the tables for monoenergetic electrons published by Berger (10) and the negatron emission spectra were determined using the code developed by Baker (11). The value of P_{90} was calculated from the scaled absorbed dose distribution.

The scaled absorbed dose distribution function falls to almost zero at a distance of $2P_{90}$, and the P_{90} values for the above radioisotopes are 0.517, 0.0822, 0.0569, and 0.0276 cm, respectively.

Consider the situation in which neoplastic cells are suspended within the CSF and radionuclide is targeted to the cell using highly specific antibody. For an isotope such as ^{90}Y with a maximum range of about 1.0 cm, only 5% of the β spectrum energy will be absorbed in a sphere of radius 0.02 cm around the point of emission. This is far greater than the radius of a cell and consequently very little energy will be deposited within the cell. Effective energy deposition within the cell can be obtained only via a cross-fire effect, indicating a volume distribution requirement for ^{90}Y. Similar arguments apply to the shorter range isotopes. Furthermore, the probability of a β particle depositing energy within a cell depends also on the direction of emission and, as discussed by Humm (9), the implied solid geometry of the binding site and the cell. Unless a short range emitter is used and is actually situated within the cell or a large number of the emitters are sited on the cell surface, cross-fire will remain an important factor in delivering a high radiation dose to the cell.

The dosimetry models previously outlined will therefore be applied to the following situations: (*a*) volume distributions for nontargeted radionuclide therapy of cells in the CSF in CNS leukemia relapse; (*b*) surface distribution of antibody targeted radionuclide therapy in leptomeningeal disease as used by Lashford *et al.* (6).

Volume Distributions. The dose rate distributions over the cross-section of the cylindrical annulus representing the spinal cord and CSF (12) (inner and outer radii, 0.5 and 0.8 cm, respectively) for a uniform distribution of the radioisotope, *i.e.*, uniform over dimension $2P_{90}$ along the spinal axis, are shown in Fig. 2. The asymmetry for the ^{90}Y distribution is due to the comparability of the cylindrical dimensions to the maximum

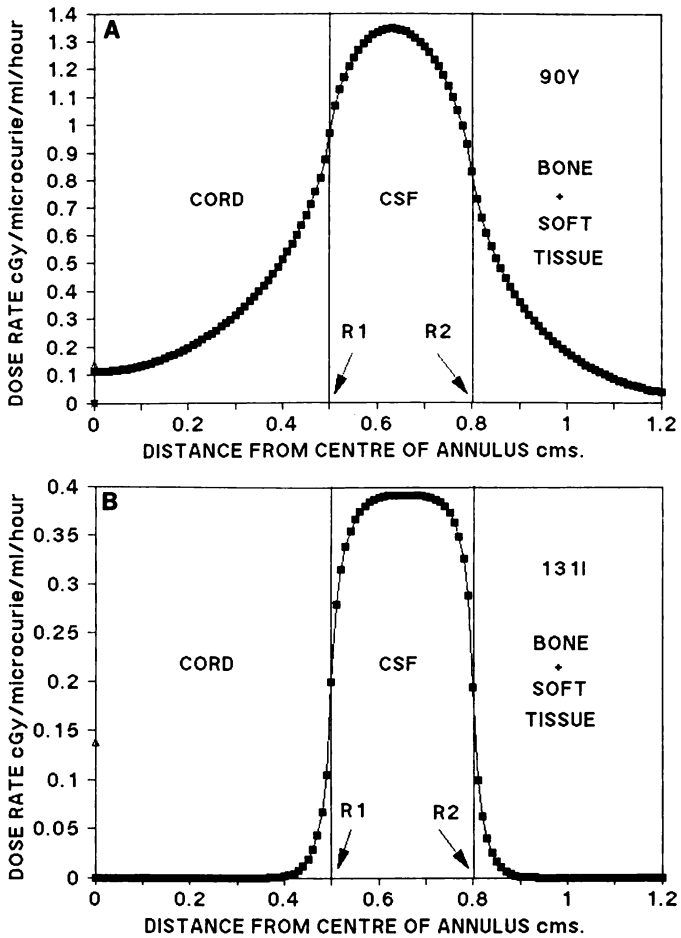

Fig. 2. Dose rate profile for homogeneous volume distribution of radionuclide activity within the CSF. *A*, ^{90}Y; *B*, ^{131}I.

range of the β emission. In order to compare the relative merits of the radionuclides, it is useful to calculate the dose rate ratio (which is equivalent to the dose ratio) defined by

$$\text{Ratio} = \frac{\text{Dose rate } (x, t)}{\text{Dose rate (0.01 cm from the inner surface)}}$$

or

$$\text{Ratio} = \frac{\text{Dose rate } (x, t)}{\text{Dose rate (0.02 cm from the inner surface)}}$$

Since the edge of the cord lies between 0.01 and 0.02 cm from the inner surface, these ratios reflect the edge of cord dose rate relative to a defined dose rate in the CSF. It can be seen that although the ^{90}Y is confined to the CSF, the relative dose rate to the cord is highly comparable to the dose rate in the CSF (Figs. 3 and 4). The average dose rate to the cord was also calculated and is reported in Table 1.

$$\text{Av. dose rate } (t) = \frac{2}{R1^2}\int_0^{R1} DR(x, t) \times dx$$

^{90}Y gives a high dose to the edge of the cord and the average dose to the cord is highly significant. As the β particle range decreases, the average cord dose and the dose ratios decrease markedly.

The nerve roots leaving the cord in the lumbar region have a radius of approximately 0.05 cm. The average dose rate to the roots (over the root cross-section) at the center of the CSF are shown in Table 2. For ^{90}Y, the dose rate will be approximately the same as in the CSF. As the radius of the nerve root decreases, the average dose rate will tend towards the dose rate in the CSF and therefore other nerve roots may receive higher dose rates. The dose rate to the dorsal and ventral nerve roots may be of less importance than the dose rate to the cord due to their relatively low radiation sensitivity.

The dose rate distribution for ^{90}Y using an annulus with inner and outer radii of 0.4 and 0.9 cm was also determined. The maximum dose rate in the CSF is slightly larger than would be

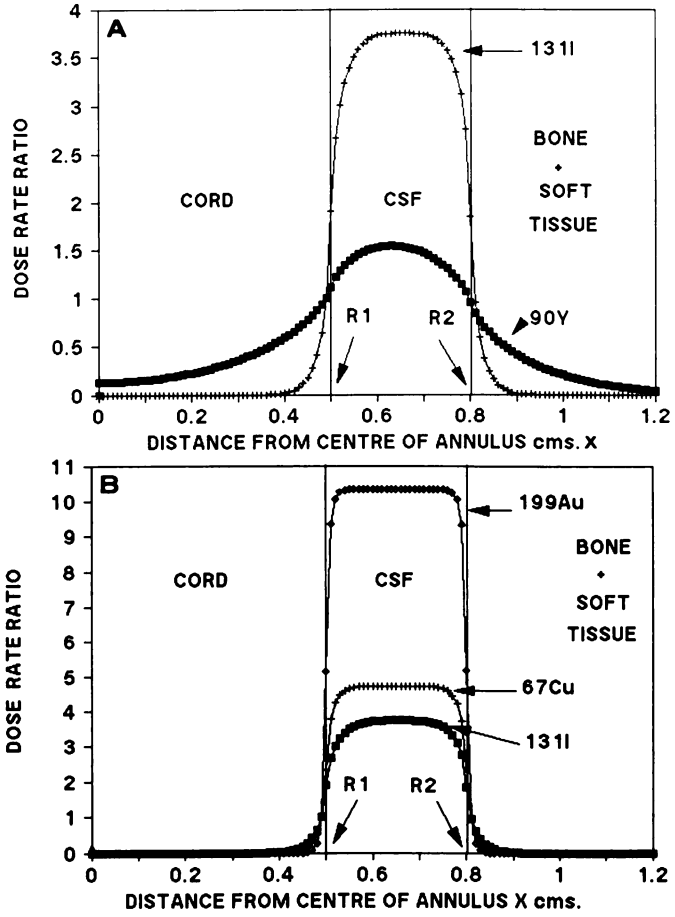

Fig. 3. Homogeneous distribution of radionuclide within the CSF volume. The dose rate ratio is the dose rate at point x expressed as a fraction of the dose rate at 0.01 cm from the inner radius at $R1$. *A*, ^{131}I and ^{90}Y; *B*, ^{67}Cu, ^{199}Au, and ^{131}I.

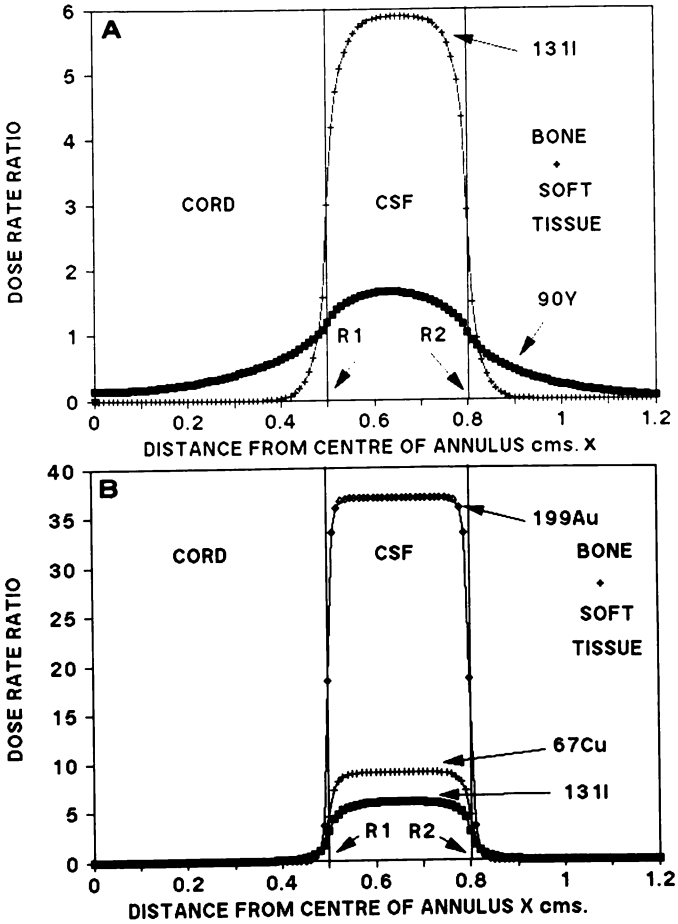

Fig. 4. As for Fig. 3 with the dose rate at point x expressed as a fraction of the dose rate at 0.02 cm from the inner radius $R1$. *A*, ^{131}I and ^{90}Y; *B*, ^{67}Cu, ^{199}Au, and ^{131}I.

Table 1 *Spinal cord*

Ratio 1 = Average dose to the cord/maximum dose in the CSF. Ratio 2 = Average dose to the cord/dose at the edge of the CSF (at $R1$).

	Ratio 1	Ratio 2
^{90}Y	0.34	0.45
^{131}I	0.037	0.074
^{67}Cu	0.026	0.052
^{199}Au	0.013	0.027
Volume distribution		

Table 2 *Nerve roots*

Ratio = Average dose to the nerve root/maximum dose in the CSF.

	Ratio
^{90}Y	Approx. 1.0
^{131}I	0.35
^{67}Cu	0.25
^{199}Au	0.13
Volume distribution	

obtained for the smaller annulus. This effect is due to the range of the β particle emission being greater than the separation between the two cylinders. Thus the dose rate is slightly dependent on the dimensions of the cylinders used to describe the model although this is not the case for the other radionuclides considered.

Surface Area Distributions. The results for surface area distributions are shown in Fig. 5. As previously noted, the dose rate computation becomes unstable at the surface and so D_{max} was taken to be the dose rate at 0.0025 cm from the surface which is a useful practical limit since this reflects the dose rate about 1 cell diameter distant from the surface. At closer distances the distribution of the radionuclide would no longer appear uniform. Dose ratios were also calculated as for the volume model (Fig. 6), as were the average dose rate to the cord (Table 3).

Since the concept of an infinitely thin distribution of radionuclide is of doubtful validity, it may be more appropriate to consider the distribution to be represented by a cylindrical annulus with a thin but finite separation between the surfaces. In order to investigate this hypothesis, a cylindrical annulus of 0.8 cm outer radius ($R2$) and 0.7975 cm inner radius ($R1$) were considered. To maintain the same activity/unit length

$$\pi(R2^2 - R1^2)Av = 2\pi R1As$$

where Av is the unit activity/unit volume and As is the unit activity/unit area. Thus, if As = 1.0 μCi/cm^2 then Av = 400 μCi/ml. These dimensions were used in both models and the calculated dose rates found to agree very closely. However, a very large number of subintervals were required in the numerical integration program for the surface distribution to minimize computational error. The volume model also implies a finite maximum dose rate which occurs at the center of the separation between the two cylinders.

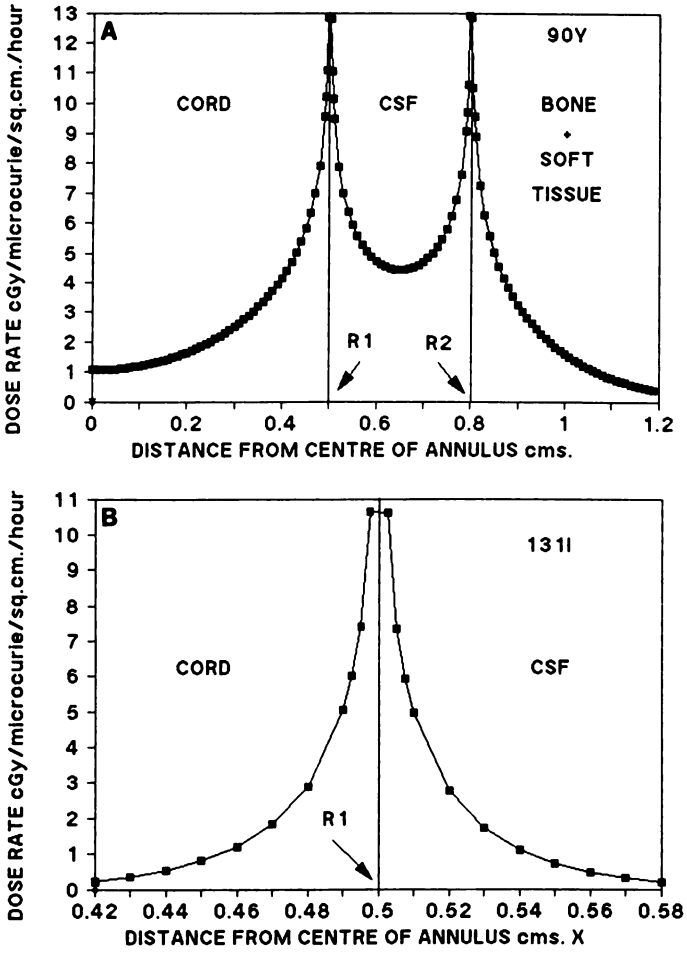

Fig. 5. Uniform distribution of radionuclide activity on the cylindrical boundary surfaces encompassing the CSF, *i.e.*, surface distribution. Maximum dose rate is at 0.0025 cm from surface. No activity is present within the CSF volume. The dose rate in the CSF is due solely to β particle emission from the surfaces of radii $R1$ and $R2$. *A*, ^{90}Y; *B*, ^{131}I.

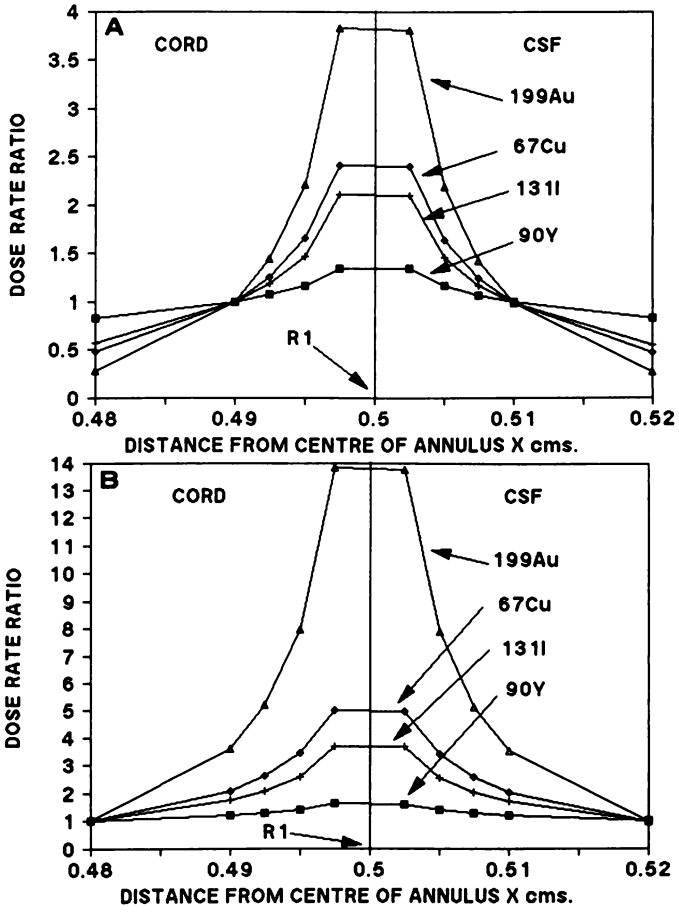

Fig. 6. Uniform surface distribution of radionuclide. The dose rate ratio is the dose rate at point x expressed as a fraction of the dose rate at 0.01 cm (*A*) and 0.02 cm (*B*) from the inner surface at radius $R1$.

Table 3 *Spinal cord*

Ratio = Average dose to the cord/maximum dose (0.02 cm from surface).

	Ratio
^{90}Y	0.31
^{131}I	0.066
^{67}Cu	0.051
^{199}Au	0.032
Surface distribution	

Discussion

^{90}Y has no γ emission and consequently cannot be imaged postinjection except by bremmstrahlung scanning. Coupled with the high dose rate to the cord resulting from therapeutic levels in the CSF, these results suggest that ^{90}Y is inappropriate for CSF directed therapy. The data presented suggest that if ^{131}I, ^{67}Cu, or ^{199}Au were used, then the average dose to the cord would be limited to between 0.074 and 0.03 of the therapeutic levels at the edge of the CSF for a volume distribution (*i.e.*, nontargeted) with almost identical factors for targeted leptomeningeal surface dose distributions (taking the dose at 0.0025

cm as the maximum therapeutic dose). Consequently, a high therapeutic target/nontarget ratio can be achieved using short range β particle emitters coupled to nontargeting carriers in the treatment of CNS leukemia. The prime requirements for this type of therapy would therefore be the development of radiolabeled carriers with minimal leakage from the CSF and maximum radionuclide/carrier stability. It is interesting to note that the dose ratio profiles (*i.e.*, dose rate/dose rate at 0.02 cm from the inner surface) are almost identical with the CSF for both volume and surface distributions. However, unlike surface dose distributions, a volume distribution would deliver a high dose to cells within the CSF. For the radionuclides discussed (except ^{90}Y), the variation in cylindrical dimensions modeling the cord/CSF will have virtually no effect on the dose rates calculated as a function of the distance from the cylindrical surfaces.

Ideally it would be desirable to give a pretherapeutic injection of the radionuclide/carrier. This would enable the kinetics of the radionuclide and the resultant dosimetry to be determined and planned prior to therapeutic administration. ^{131}I, ^{67}Cu, and ^{199}Au have suitable γ emissions for imaging and would therefore be the radionuclides of choice. Therapeutic restrictions may be imposed by the dose to other nontarget tissues due to leakage/dissociation of the radionuclide-carrier complex, although this could be determined by the pretherapy imaging provided the pretherapy and therapy radiopharmaceuticals were identically prepared.

The benefits of short range β-emitting radionuclides would suggest that α particle emitters, *e.g.*, ^{211}At and ^{212}Bi, could be utilized for therapy. However, these radioisotopes have a relatively short half-life (8 and 1 h). The slow CSF flow rate, some aspects of the structure of the spinal canal (crevices), and the time required for adequate mixing would appear to preclude their use. The preinfusion of streptavidin labeled antibodies (13) and the introduction of astatinated biotin after equilibration may be a possible solution to this problem. Some of these difficulties could be circumvented by using boron labeled carriers and, after a suitably long period of time for adequate equilibration, activating the boron with an external beam of neutrons (boron neutron capture therapy) (14).

Appendix 1

The dose rate at point P (situated such that the length of the cylinder above and below the point is $2P_{90}$) due to a point S in the cylinder volume is (Fig. 7)

$$DR(x, R1, t) = 2\Delta A(t) \int_v \Phi(R)\, dV$$

where V is the volume of the cylinder above the x,y plane (*i.e.*, $z \geqq 0$). Using spherical coordinates, P as the axes origin, and $\zeta = R/P_{90}$

$$DR(x, R1, t) = 2\ \Delta A(t) \int_v \Phi(R) R^2 \sin\phi\, dR\, d\theta\, d\phi$$

$$= \frac{\Delta A(t)}{2\pi P_{90}} \int_v F(\zeta) \sin\phi\ dR\, d\theta\, d\phi$$

$$= -\frac{\Delta A(t)}{2\pi P_{90}} \int_{\theta_1}^{\theta_2} d\theta \int_{R_a}^{R_b} dR\, F(\zeta)[\cos\phi]_{\phi_1}^{\phi_2}$$

where $[\cos\phi]_{\phi_1}^{\phi_2} = \cos\phi_2 - \cos\phi_1$. It can be shown that if S is on the surface

$$(D - R \sin\theta \sin\phi)^2 + R^2 \sin^2\phi \cos^2\theta = R1^2$$

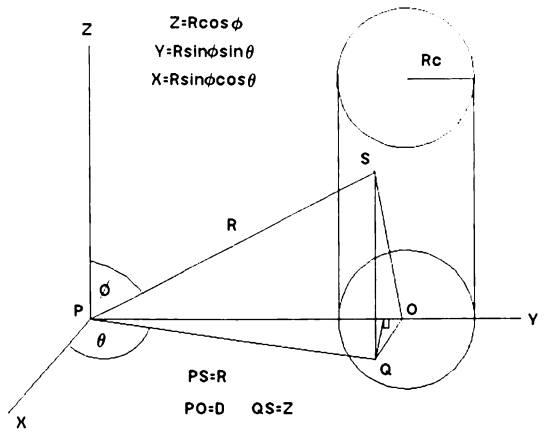

Fig. 7. Coordinate system used for calculating the dosimetry due to a distribution of radionuclide within the CSF volume.

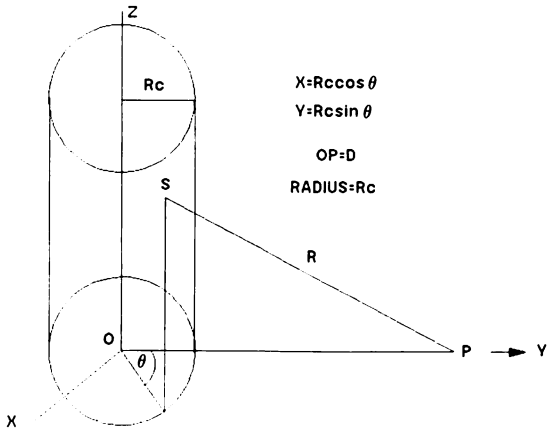

Fig. 8. Coordinate system used for calculating the dosimetry due to a distribution of radionuclide on the cylindrical surface.

and

$$\sin\phi = \frac{1}{R1}\left(D \sin\theta \pm (R1^2 - D^2\cos^2\theta)^{0.5}\right)$$

from which cos ϕ can be calculated. The roots of this equation give ϕ_1 and ϕ_2 where ϕ_1 has the negative option and ϕ_2 has the positive option.

Limits of Integration. If $D \geqq R1$ then

$$R_a = D \sin\theta - (R1^2 - D^2\cos^2\theta)^{0.5}$$

$$R_b = 2P_{90}$$

$$\theta_1 = \cos^{-1}(R1/D)$$

$$\theta_2 = \pi - \theta_1$$

If $\cos^2\phi < 0$ then $\cos\phi = 0$. If $\cos^2\phi > 1.0$ then $\cos\phi = 1.0$. Otherwise ϕ_1 and ϕ_2 are as previously defined. If $D < R1$ then

$$\theta_1 = -\pi/2$$

$$\theta_2 = \pi/2$$

If $\cos^2\phi < -1.0$ then $\cos\phi = -1.0$. If $\cos^2\phi > 1.0$ then $\cos\phi = 1.0$. The limits R_a and R_b are as before. If $R = D$ then

$$\theta_1 = 0$$

$$\theta_2 = \pi$$

Appendix 2

The dose rate at point P due to all points S on the surface is (Fig. 8)

$$DR(x, R1, t) = \Delta\ A(t) \int_s \Phi\ (R)\ ds$$

where S is the surface area of the cylinder.

$$DR(x, R1, t) = \frac{2\Delta A(t)}{4\pi P_{90}} \int_{\theta_1}^{\theta_2} \int_{z_1}^{z_2} \frac{F(\zeta)}{R^2} R1 \, d\theta \, dz$$

where $\zeta = R/P_{90}$ and

$$R^2 = D^2 + R1^2 - 2 D R1 \sin\theta + z^2$$

The integration limits are

$$\theta_1 = 0$$

$$\theta_2 = 2\pi$$

$$z_1 = 0$$

$$z_2 = (4 P_{90}^2 + 2 D R1 \sin\theta - D^2 - R1^2)^{0.5}$$

References

1. Epenetos, A. A., Munro, A. J., Stewart, S., Rampling, R., Lambert, H. E., McKenzie, C. G., Soutter, P., Rahemtulla, A., Hooker, G., Sivolapenko, G. B., Snook, D., Courtenay-Luck, N., Dhokia, B., Krausz, T., Taylor-Papadimitriou, J., Durbin, H., and Bodmer, W. Antibody-guided irradiation of advanced ovarian cancer with intraperitoneally administered radiolabelled monoclonal antibodies. J. Clin. Oncol., *5:* 1890–1899, 1987.
2. Carrasquillo, J. A., Krohn, K. A., Beaumier, P., McGuffin, R. E., Brown, J. P., Hellström, E., Hellström, I., and Larson, S. M. Diagnosis of and therapy for solid tumours with radiolabelled antibodies and immune fragments. Cancer. Treat. Rep., *68:* 317–328, 1984.
3. Order, S. E. Isotopic immunotherapy: radiolabelled antibody. Int. J. Radiat. Oncol. Biol. Phys. *14:* S77–S81, 1988.
4. Desphande, S. V., DeNardo, S. J., Meares, C. F., McCall, M. J., Adams, G. P., Moi, M. K., and DeNardo, G. L. Copper-67-labelled monoclonal antibody Lym-1, a potential radiopharmaceutical for cancer therapy: labelling and biodistribution in RAJI tumoured mice. J. Nucl. Med. *29:* 217–225, 1988.
5. Freeman, A. I., and Mayhew, E. Targeted drug therapy. Cancer (Phila.), *58:* 573–583, 1986.
6. Lashford, L. S., Davies, A. G., Richardson, R. B., Bourne, S. P., Bullimore, J. A., Eckert, H., Kemshead, J. T., and Coakham, H. B. A pilot study of ^{131}I monoclonal antibodies in the therapy of leptomeningeal tumours. Cancer (Phila.), *61:* 857–868, 1988.
7. Vaughan, A. T. M., Anderson, P., Dykes, P. W., and Bradford, A. R. Limitations to killing of tumours using radiolabelled antibodies. Br. J. Radiol., *60:* 567–578, 1987.
8. Berger, M. J. Distribution of absorbed dose around point sources of electrons and β particles in water and other media. MIRD Pamphlet No. 7. J. Nucl. Med., Suppl. 5.
9. Berger, M. J. Improved point kernels for electron and beta ray dosimetry. Nat. Bur. Stand. Report NBSIR 73-107, Feb. 1973.
10. Baker, L. J. The calculation of spectra and effective energies of beta decay. AERE-R10306, May 1982.
11. Humm, J. L. Dosimetric aspects of radiolabelled antibodies for tumour therapy. J. Nucl. Med. *27:* 1490–1497, 1986.
12. Truex, R. C., and Carpenter, M. B. Human Neuroanatomy. Baltimore: Williams & Wilkins Company, 1969.
13. Hnatowich, D. J., Virzi, F., and Rusckowski, M. Investigations of avidin and biotin for imaging applications. J. Nucl. Med. *28:* 1294–1302, 1987.
14. Barth, R. F., Johnson, C. W., Wei, W. Z., Carey, W. H., Soloway, A. H., and McGuire, J. Neutron capture therapy using boronated monoclonal antibodies against tumour associated antigens. Cancer Detect. Prevent., *5:* 315, 1982.